Sahakian, V.J., Derosier, B.J., Rockwell, T.K., and Stock, J.M., 2022, Shallow distributed faulting in the Imperial Valley, California, USA: Geology, v. 50, https://doi.org/10.1130/G49572.1

Supplemental Material

Shallow Distributed Faulting in the Imperial Valley

Valerie J. Sahakian, Boe Derosier, Thomas Rockwell, and Joann M. Stock

Supplemental Information Text 1: Methods

Seismic Data

Acoustic compressed high-intensity radar pulse (CHIRP) images sub-surface sediments with decimeter resolution, by coupling acoustic energy in a swept frequency pulse with water. Using two trucks on the opposite levees of the AAC (Figure 2), we towed an Edgetech SubScan JSTAR CHIRP 512 with a dual transducer XStar sonar West to East through the canal in a floating cage. We used a 50ms 0.7–3.0kHz pulse, and placed a Septentrio Altus NR3 GNSS instrument on top of the CHIRP with a 1Hz sample rate to obtain real-time, sub-meter positioning on the seismic data.

We applied a time-varying gain to increase the clarity and coherency of deeper reflectors. We convert two-way travel time (TWTT) to depth assuming a water velocity of 1350-1500m/s, but only show conversions with 1500 m/s here, as they demonstrate the best correlative relationship with strata observed in nearby terrestrial cores. Depth penetration varied between survey regions, between 10 and 25m beneath the subsurface.

^{14}C Dating and Sedimentation Rate

We approximate ages of the sediments by estimating two average regional sedimentation rate, as sedimentation here is episodic. This is a highly approximate endeavor, and we do not aim to use our findings here with any certainty but rather, to provide very approximate temporal constraints on our seismic images.

For age constraints, we use the most reliable ^{14}C dates on samples recovered from nearby cores from Rockwell & Klinger (2019), and apply it to deep sediments below Lake G. This study produced two deep cores along a CPT profile, an eastern and a western core with ^{14}C dates recovered from samples within, calibrated using OxCal (Ramsey, 2008). Calibrations were performed with an R value of 0, which is not well-constrained and partially arbitrary.

We cannot directly corroborate reflectors with units from these cores. Instead, we estimate the ages of sediments in three main steps:

1. Assume sediments <5m depth are likely younger than Lake F (the base of Lake F is ~5m depth when accounting for the 1m high berm through which the core was drilled), and obtain an age estimate from Philibosian et al. (2011) of about 1100 years BP.
2. Compute an approximate sedimentation rate for sediments between ~5m and 8m depth to the base of Lake G, dated at the Dogwood paleoseismic site (Rockwell et al., 2011), and 9m depth, corresponding roughly to the sediments below Lake G that are dated by sample

E7 from Rockwell & Klinger (2019). *For reflectors in this depth range, we add the age of Lake F to the corresponding age assuming this intermediate sedimentation rate.*

3. Compute an approximate sedimentation rate for sediments at 11-12m depth, using samples E7 and E4 (recovered from another lake level below Lake G) from Rockwell & Klinger (2019). We add the age of ~10m deep sediments from step 2 to the corresponding age of the additional depth of sediments with this deeper sedimentation rate.

A note on the samples used in constraining sedimentation rate: The Rockwell & Klinger (2019) eastern core samples a regional sag, but presents the most reliable radiocarbon dates (samples E7 and E4 at 20.9m and 24m depth, respectively, in the eastern core). The western core is most similar to the depositional environment in the regions of our profiles, and where we think we can best correlate units with reflectors in our data. Units can, however, be correlated between the eastern and western cores; sample E7 is derived from unit 850, and E4 corresponds to unit 1000. Both are below (and thus older) than Lake F, and within the western core are at 9.0-9.8m and 11.6m depth, respectively (Table S1).

Step 2, "Intermediate" Sedimentation Rate: We compare sedimentation between the Lake F unit (unit 700), and unit 850. We obtain the date for unit 850 from sample E7 from Rockwell & Klinger (2019), and the depth from samples W6 and W5 (corresponding samples for unit 850 in the western core). We obtain a reliable age estimate for the Lake Cahuilla highstand Lake F from Philibosian et al. (2011). Here, Lake F is Layer 6L, and calibrated dates are presented, ~1.1 – 1.2ka (Table S1). Using this calibrated range, we obtain a minimum and maximum sedimentation rate between the appropriate Lake F unit depth of 5m in the western core of Rockwell & Klinger (2019), and the depths of samples W5 and W6. The minimum sedimentation rate (minimum difference in depth divided by maximum difference in age) yields 4m in 1100 years, or 3.6m/kyr. The maximum sedimentation rate (maximum sedimentation, minimum age difference) yields 4.5m in 836 years, or 5.7m/kyr.

Step 3, "Deeper" Sedimentation Rate: We compute a minimum and maximum sedimentation rate between units 850 and 1000, using the calibrated radiocarbon dates for samples E7 and E4 and their corresponding depths in the western core. The minimum sedimentation rate is determined from the minimum depth range between samples W7 and W5, and maximum age difference based on the asymmetric calibrated dates, and yields 1.8m in 392 years, or 4.6m/kyr. The maximum sedimentation rate is determined from the maximum depth range between samples W7 and W6, and minimum age difference, and yields 2.6m in 137 years, or 19m/kyr. These are thus reported as the "average" sedimentation rate range: 4.6 – 19 m/kyr for deeper sediments, below ~10m.

Determining Ages of Reflectors: We are interested in the approximate ages of several reflectors. The first is at ~9.5 – 14.5m below sea level. We cannot directly corroborate units and depths between the cores and our profile. Instead, we assume the first ~5m of sediment are younger than Lake F (1.1 – 1.2ka), and the remaining 4.5 were deposited under the younger sedimentation rate (3.6 – 5.7m/kyr). Sediments at 9.5m depth are ~1.9 to 2.5ka. Sediments at ~10m depth are ~2 to 2.6ka. Sedimentation becomes more highly variable after this, so we apply the deeper, "average" sedimentation rate for the remaining 4.5m of sediment, resulting in an approximate age of 2.2 to 3.6ka. For the depth range 9.5 – 14.5m, we thus present a possible age

range of ~1.9 to 3.6ka. Reflectors at ~0.0125s two-way travel time (TWTT) are at approximately 9.4m depth, thus corresponding to an age of <2.5ka, as described above.

Lastly, we note that this process is highly uncertain and prone to errors due to the nature of assumptions in the above process, as well as water velocity assumptions in converting our observations of TWTT to depth. The above ages are meant to place very approximate (Holocene or Pleistocene) constraints on our observed strata.

Interpretations

We qualitatively characterize our faulting and deformation interpretations as "confident" (obvious offset in a reflector, usually with adjacent deformation of reflector(s)) "medium confidence" (moderate clarity, and/or deformation likely controlled by a fault structure, but no clear offsets present) and "uncertain" (low clarity, variability in character of reflectors but no clear warping of adjacent reflectors and no clear offsets). The top ~0-5m of many seismic lines show bright reflectors indicating fluvial bedforms, produced by unidirectional westward flow of the canal current (Southard et al., 1991).

Coulomb Stress Models

We test the possibility that seismicity is absent in the Michoacán/Dixieland faults stepover due to a stress shadow from previous large earthquakes with simple models of coulomb stress change (Figures S9, S10) in the region from the 1979 Imperial Valley earthquake, and 2010 El Mayor-Cucapah earthquakes. We use the Coulomb 3.4 package (Toda et al., 2005; Lin et al., 2004). With the source models of Archuleta et al (1984) and Wei et al. (2011), we compute the coulomb stress change on regional receiver faults of strike 324, 317, 313, and 312 (the strike of the IF, WF, DF, and MF, respectively), assuming the strike of the features we observe are similar to the above. The dip is assumed to be 90 degrees for all. We compute the static stress change on these receiver faults at 7.5km depth, and with a Poisson's ratio of 0.25, friction coefficient of 0.4, and Young's Modulus of 80 GPa.

We additionally consider the possibility that the receiver faults may not be entirely vertical. Although the Southern California Earthquake Center Community Fault Model (SCEC CFM, Nicholson et al., 2020; Plesch et al., 2020) presents the dip of all the above faults as 90 degrees, Persaud et al. (2016) show seismicity lineaments of the Weinert-El Centro fault that graphically (not described within the manuscript) feature an approximately 56 degree dip to the northeast. We thus compute the coulomb stress change for the Archuleta et al. (1984) model on receiver faults of strike 324, dip 56 degrees; and 313, dip 56 degrees, as end members. We choose the Archuleta model as opposed to the Wei model to test this hypothesis as it demonstrates the closest difference in positive vs. negative Coulomb stress change near our study of interest. We find no demonstrable differences within our stepover of interest in this case, and thus do not present it here.

References:

Archuleta, R. J. (1984). A faulting model for the 1979 Imperial Valley earthquake. *Journal of Geophysical Research: Solid Earth*, *89*(B6), 4559-4585.

Lin, J. and R.S. Stein, 2004, Stress triggering in thrust and subduction earthquakes, and stress interaction between the southern San Andreas and nearby thrust and strike-slip faults, Journal of Geophysical Research,, v. 109, B02303, doi:10.1029/2003JB002607.

Nicholson, C., Plesch, A., Sorlien, C. C., Shaw, J. H., & Hauksson, E. (2020, 08). Updates, Evaluation and Improvements to the Community Fault Model (CFM version 5.3). Poster Presentation at 2020 SCEC Annual Meeting. SCEC Contribution 10412

Persaud, P., Ma, Y., Stock, J. M., Hole, J. A., Fuis, G. S., & Han, L. (2016). Fault zone characteristics and basin complexity in the southern Salton Trough, California. *Geology*, *44*(9), 747-750.

Philibosian, B., Fumal, T., & Weldon, R. (2011). San Andreas fault earthquake chronology and Lake Cahuilla history at Coachella, California. *Bulletin of the Seismological Society of America*, *101*(1), 13-38.

Plesch, A., Marshall, S. T., Nicholson, C., Shaw, J. H., Maechling, P. J., & Su, M. (2020, 08). The Community Fault Model version 5.3 and new web-based tools. Poster Presentation at 2020 SCEC Annual Meeting. SCEC Contribution 10547

Ramsey, C. B. (2008). Deposition models for chronological records. *Quaternary Science Reviews*, *27*(1-2), 42-60.

Rockwell, T., & Klinger, Y. (2019). Testing Recurrence Models for a Simple Plate Boundary Fault: Continuation of a Paleoseismic Study of the Imperial Fault in the Region of Large 1940 Displacement. USGS EHP Grant # G18AP00004 Final Report.

Southard, J. B. (1991). Experimental determination of bed-form stability. *Annual Review of Earth and Planetary Sciences*, *19*(1), 423-455.

Toda, S., R. S. Stein, K. Richards-Dinger and S. Bozkurt, 2005, Forecasting the evolution of seismicity in southern California: Animations built on earthquake stress transfer, Journal of Geophysical Research, v. 110, B05S16, doi:10.1029/2004JB003415.

*Table S1 – Table of samples, units, and dates used in constraining sedimentation rate. *Indicates samples from Rockwell et al., (2019); ** Indicates samples from Philibosian et al., 2011. Calibrated ages are from Philibosian et al. (2011), Figure 15, sample Nb4m13A-c.*
[†] Indicates the corresponding unit as described by Rockwell et al., 2019.

Sample	Depth (m)	Unit	^{14}C (BP)	± (years)	Calibrated Age	Equivalent Western Core Sample	Equivalent Western Core Depth (m)
Nb4m13A-c (Layer 6Lb SW)**	-	700[†]	1080-1185 (1.151 – 1.256 ka)	15-30	795 – 900 AD (1.226 – 1.1121 ka)	-	5
E7*	20.9	850	2435 (2.506 ka)	20	195-41 BCE (2.216-2.062 ka)	W6	9.0
						W5	9.8
E4*	24	1000	2640 (2.711 ka)	15	433-332 BCE (2.454 – 2.353 ka)	W7	11.6

Table S2 - Locations of mapped "confident" faults from this study.

Longitude (Decimal Degrees)	**Latitude (Decimal Degrees)**
-115.60702	32.6572889
-115.60049	32.6578206
-115.54814	32.6616501
-115.54744	32.6617141
-115.54708	32.6617911
-115.54664	32.6618085
-115.53713	32.6625143
-115.53706	32.6625203
-115.53591	32.6626241
-115.36228	32.675184

Table S3 - Locations of mapped "medium" faults from this study.

Longitude (Decimal Degrees)	**Latitude (Decimal Degrees)**
-115.61377	32.6568383
-115.61358	32.6568678
-115.5996	32.6578761
-115.53804	32.6624031
-115.36081	32.6753023
-115.35662	32.6754888
-115.51481	32.686402

Table S4 - Location of mapped "uncertain" faults from this study.

Longitude (Decimal Degrees)	**Latitude (Decimal Degrees)**
-115.60957	32.6571436
-115.60269	32.6576489
-115.59803	32.657942
-115.59805	32.6579444
-115.59187	32.6584299
-115.54087	32.662215
-115.3593	32.6753931
-115.35831	32.6754253
-115.3584	32.6754264
-115.34398	32.6764004
-115.33479	32.6774489
-115.32907	32.679028
-115.49566	32.6864354

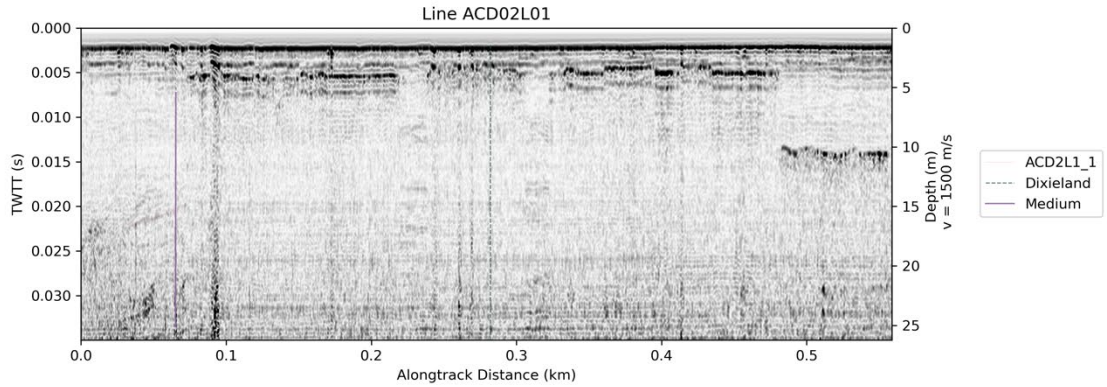

Figure S1 – Interpreted line ACD02L01, Day 2 Line 1 in Region 2, crossing the Dixieland fault. Plotted as TWTT versus alongtrack distance, and depths reported on the right-hand side axis are computed assuming a nominal water velocity of 1500m/s. Interpretations include horizon mapped on this line (ACD2L1_1), the mapped trace of the Dixieland fault from the Southern California Earthquake Center Community Fault Model, and a "medium" certainty mapped fault from this study.

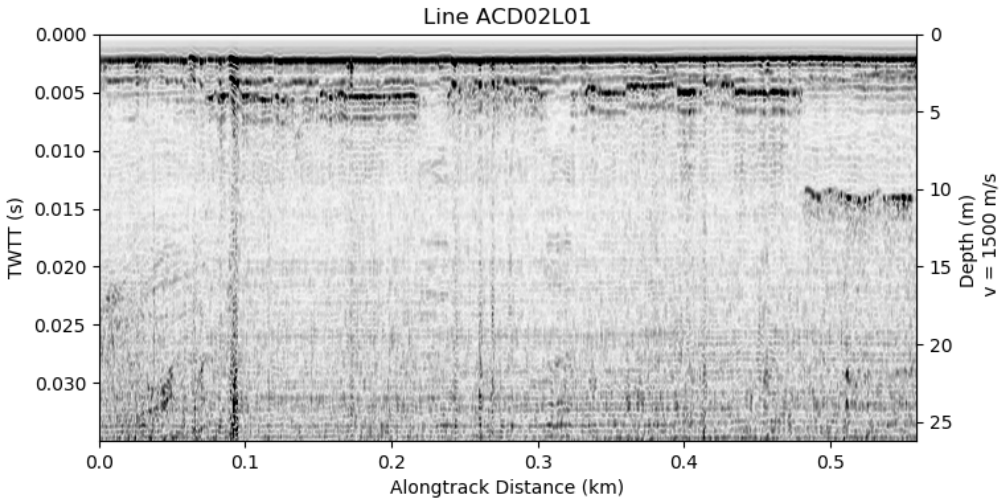

Figure S2 - Uninterpreted line ACD02L01, Day 2 Line 1 in Region 2, crossing the Dixieland fault. Plotted as TWTT versus alongtrack distance, and depths reported on the right-hand side axis are computed assuming a nominal water velocity of 1500m/s.

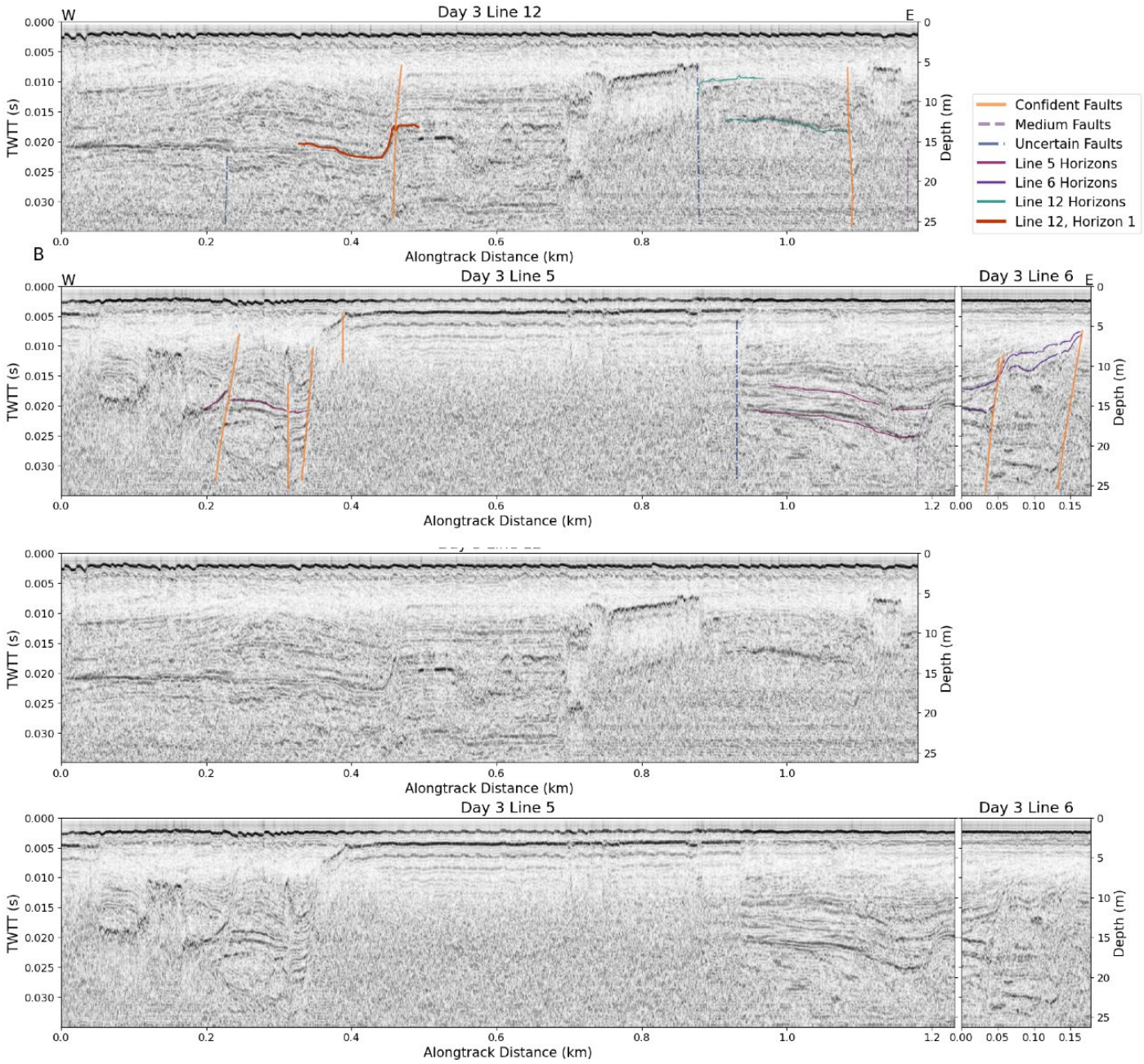

Figure S3 – Interpreted (top two panels) and uninterpreted (bottom two panels) lines ACD03L12 (Day 3 Line 12), ACD03L05 (Day 3, Line 5), and ACD03L06 (Day 3, Line 6) in Region 3. Plotted as TWTT versus alongtrack distance, and depths reported on the right-hand side axis are computed assuming a nominal water velocity of 1500m/s. Interpretations include Line 5, Line 6, and Line 12 Horizons, as well as notable Horizon 1 on Line 12. Also included are "confident", "medium", and "uncertain" mapped structures from this study.

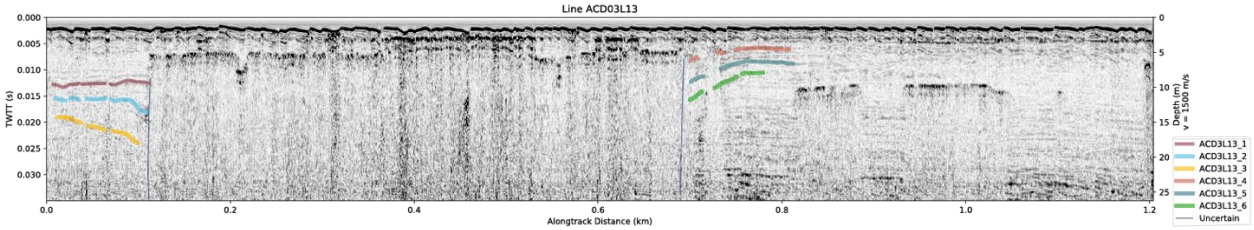

Figure S4 - Interpreted line ACD03L13, Day 3 Line 13 in Region 3. Plotted as TWTT versus alongtrack distance, and depths reported on the right-hand side axis are computed assuming a nominal water velocity of 1500m/s. Interpretations include 6 horizons ("ACD03L13_1" through "_6"), and "uncertain" mapped structures from this study.

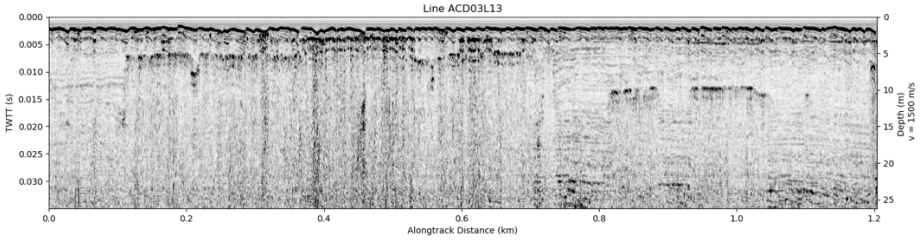

Figure S5 - Uninterpreted line ACD03L13, Day 3 Line 13 in Region 3. Plotted as TWTT versus alongtrack distance, and depths reported on the right-hand side axis are computed assuming a nominal water velocity of 1500m/s.

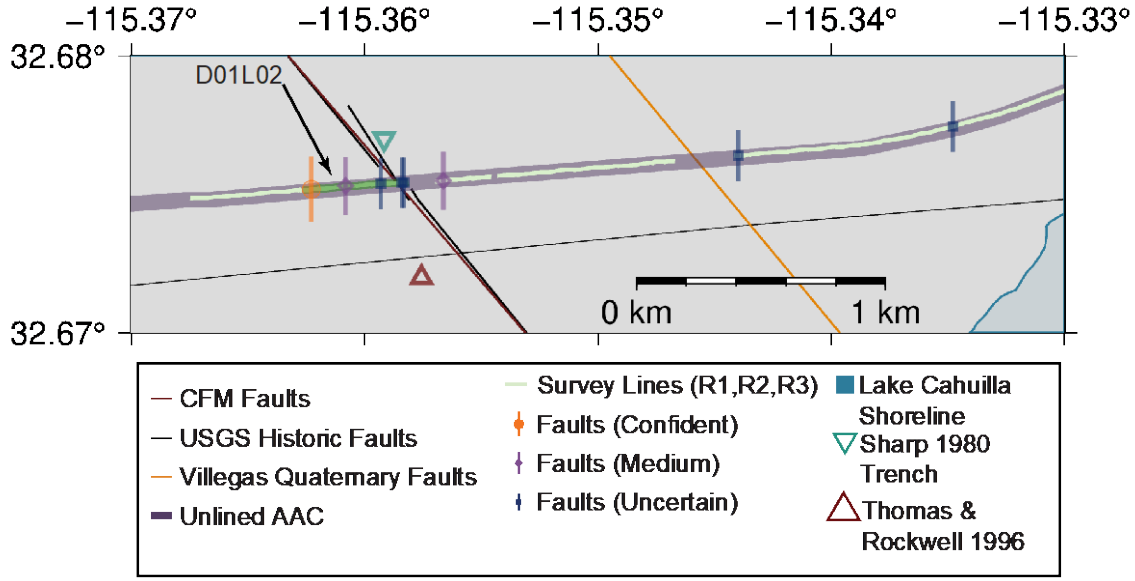

Figure S6 - Zoom-in of Figure 1, showing the Imperial Fault at the border, and respective locations of our mapped structures along with existing trenches (Sharp 1980, Thomas & Rockwell, 1996). Southern California Earthquake Center community fault model (SCEC CFM 5.3) faults (Plesch et al., 2020), US Geological Survey (USGS) historic faults (USGS, 2017), Mexico quaternary faults (Villegas et al., 2017), unlined All American Canal (AAC), trenches of Sharp (1980) and Thomas & Rockwell (1996; T&R 1996), and the ancient Lake Cahuilla

footprint (Buckles et al., 2002) are described in legend. Seismic lines presented are highlighted in green

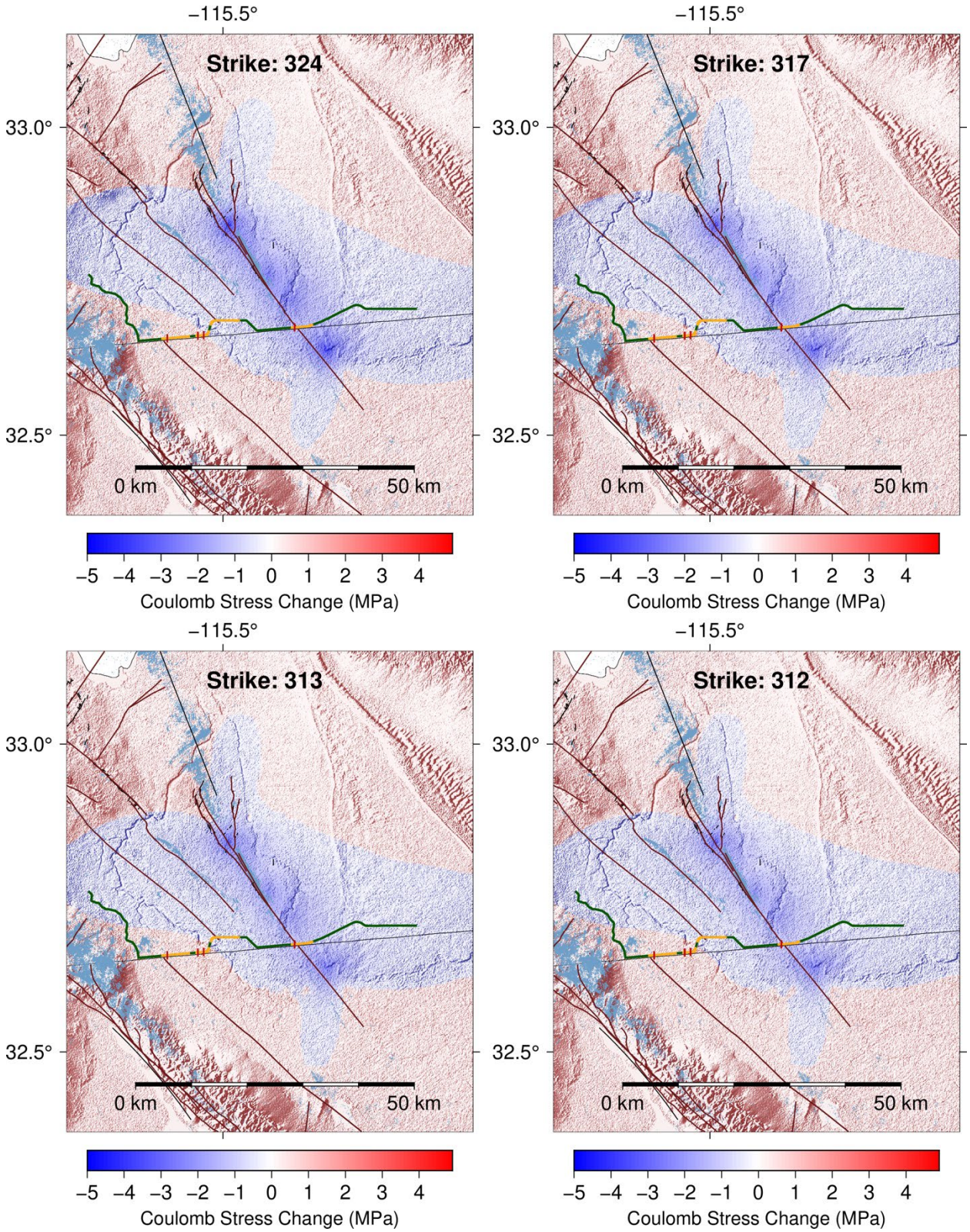

Figure S7 - Coulomb stress changes for the Archuleta et al., (1984) 1979 Imperial Valley earthquake source model on receiver faults of strike 324, 317, 313, and 312, and dip of 90 degrees.

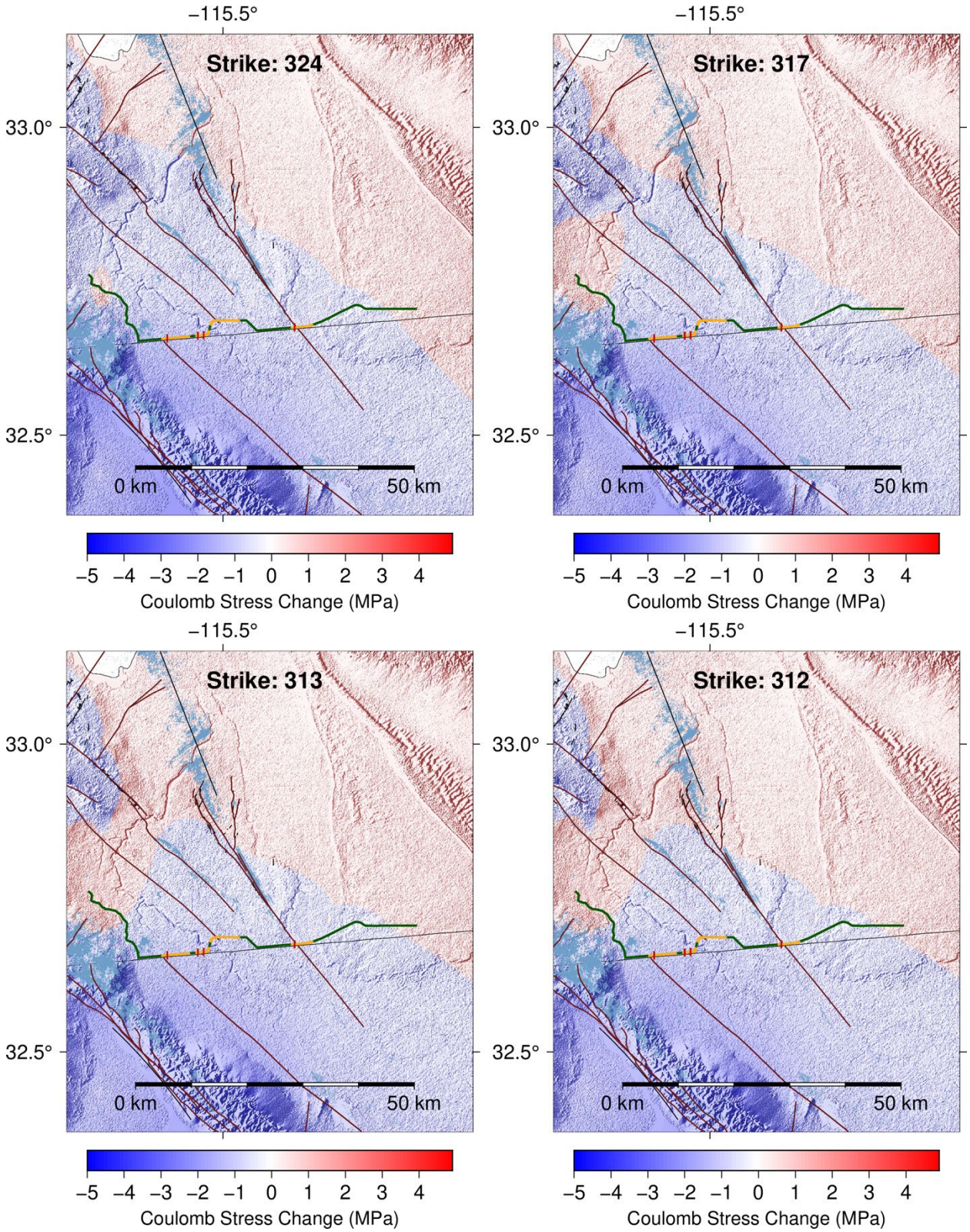

Figure S8 - Coulomb stress changes for the Wei et al., (2011) 2010 El Mayor-Cucapah earthquake source model on receiver faults of strike 324, 317, 313, and 312, and dip of 90 degrees.